Sensitivity of climate-chemistry model simulated atmospheric composition to the application of an inverse relationship between NO_x emission and lightning flash frequency

Francisco J. Pérez-Invernón[1], Francisco J. Gordillo-Vázquez[1], Heidi Huntrieser[2], Patrick Jöckel[2], and Eric J. Bucsela[3]

[1]Instituto de Astrofísica de Andalucía (IAA), CSIC, PO Box 3004, 18080 Granada, Spain
[2]Deutsches Zentrum für Luft- und Raumfahrt, Institut für Physik der Atmosphäre, Oberpfaffenhofen, Germany
[3]SRI International, Menlo Park, CA, USA

Correspondence: Francisco J. Pérez-Invernón (fjpi89@gmail.com)

Abstract. Lightning-produced nitrogen oxides (LNO_x=LNO+LNO_2) are an important source of upper tropospheric ozone. Typical parameterizations of LNO_x in climate-chemistry models introduce a constant amount of NO_x per flash or per flash type. However, recent satellite-based NO_2 measurements suggest that the production of LNO_x per flash depends on the lightning flash frequency. In this study, we implement a new parameterization of LNO_x production per flash based on the lightning flash frequency into a climate-chemistry model to investigate the upper limit implications for the chemical composition of the atmosphere. We find that a larger production of LNO_x in weak thunderstorms leads to a larger mixing ratio of NO_x in the lower and the middle troposphere, and to a lower mixing ratio of NO_x in the upper troposphere. The mixing ratios of O_3, CO, HO_x, HNO_3 and HNO_4 in the troposphere are influenced by the simulated changes of LNO_x. Our findings indicate a larger release of nitrogen oxides from lightning in the lower and the middle atmosphere, producing a slightly better agreement with the measurements of tropospheric ozone at a global scale. In turn, we obtain a small decrease of the lifetime of methane and of carbon monoxide, ranging between 0.7% and 3.4%.

1 Introduction

Nitrogen oxides (NO_x = NO + NO_2) produced by lightning in the upper troposphere (Zeldovich et al., 1947) is about 6 times more efficient in driving ozone production than anthropogenic NO_x emissions, producing about 100 molecules of ozone per molecule of lightning-produced NO_x (LNO_x) (Schumann and Huntrieser, 2007). Thus, LNO_x affects the oxidizing capacity of the atmosphere and the tropospheric budget of carbon monoxide and methane (Wu et al., 2007; Murray et al., 2012; Gordillo-Vázquez et al., 2019).

The global production of LNO_x is between 2 and 8 Tg N per year, which accounts for approximately 10% of the global NO_x sources. In the tropics, LNO_x is responsible for around 20% of the total NO_x production (Schumann and Huntrieser, 2007, and references therein). Moreover, the LNO_x Production Efficiency (PE) per lightning flash shows a large variability between different regions and thunderstorms [e. g., Pickering et al. (2016); Bucsela et al. (2019); Allen et al. (2019, 2021); Zhang et al.

(2022); Pérez-Invernón et al. (2022a)]. In particular, systematic retrievals of LNO_x from the Ozone Monitoring Instrument (OMI) by Bucsela et al. (2019); Allen et al. (2019) and the Sentinel-5P TROPOspheric Monitoring Instrument (TROPOMI) by Allen et al. (2021) reported an inverse relationship between flash rates and LNO_x PE per flash. Bucsela et al. (2021)

25 reported a new evaluation of TROPOMI-based LNO_x PE estimations by using GLM lightning measurements and a new set of atmospheric chemistry simulations to estimate the effect of the background-NO_x in the computations. According to Bucsela et al. (2021), the relationship between the production of LNO_x PE and the lightning flash frequency could be weaker than the relationship previously reported by Bucsela et al. (2019) for weak and medium active thunderstorms (thunderstorms with less than 3,000 flashes per hour and degree). Studies based on airborne measurements found a proportional relationship between

30 flash length and LNO_x PE per flash (Wang et al., 1998; Stith et al., 1999; Schumann and Huntrieser, 2007; Huntrieser et al., 2008). The inverse relationship between the length of lightning channels and the frequency of lightning occurrence in storms can reconcile these measurements (Bruning and MacGorman, 2013). Recently, Pérez-Invernón et al. (2023b) and Pickering et al. (2024) estimated LNO_x PE per flash by combining Lightning Mapping Arrays (LMA) with satellite- and aircraft-based NO_x measurements, respectively. They found that thunderstorms with larger lightning rates produce shorter flash channel

35 lengths and lower LNO_x PE per flash, confirming previous results.

Lightning parameterizations in climate-chemistry models define the emissions of LNO_x by lightning as a total number of NO_x molecules per flash, sometimes distinguishing between CG (cloud-to-ground) and IC (intra-cloud) lightning strikes by a factor of 10 (Price et al., 1997; Allen and Pickering, 2002; Tost et al., 2007; Murray et al., 2012; Jöckel et al., 2016; Gordillo-Vázquez et al., 2019; Luhar et al., 2021; Pérez-Invernón et al., 2023a) or between tropical and extratropical regions (Murray

40 et al., 2012). The parameterization of lightning and LNO_x production has a substantial impact on the global ozone burden. Specifically, these parameterizations can simultaneously lead to significant overestimates and underestimates of tropospheric ozone mixing ratios in different regions. For instance, Grewe et al. (2001) and Allen and Pickering (2002) noted that commonly used lightning parameterizations based on Cloud Top Height (CTH) can result in an underestimation of tropospheric ozone mixing ratios in the Southern Hemisphere and, conversely, an overestimation in the Northern Hemisphere. Therefore, they

45 developed a new lightning parameterizations that produce a larger lightning flash frequency over the ocean (Tost et al., 2007). More recently, Luhar et al. (2021) proposed a modification of the lightning parameterization based on the CTH by Price et al. (1997) to partially address this disagreement. The new lightning parameterization by Luhar et al. (2021) led to a larger production of LNO_x over the ocean, producing more tropospheric ozone in the Southern Hemisphere, which agrees better with observations. However, their new lightning parameterization produced an enhancement of tropospheric ozone in the Northern

50 Hemisphere, in disagreement with ozone measurements.

Previous studies have proposed various parameterizations for LNO_x production to introduce a certain level of variability and investigate the sensitivity of tropospheric chemical composition (Koshak et al., 2014; Kang et al., 2019; Wu et al., 2023). However, so far there have been no sensitivity studies of climate-chemistry models to lightning NO_x production parameterizations based on lightning frequency. In this study, we explore the differences of the chemical composition of the atmosphere by using

55 a parameterization of LNO_x production based on lightning frequency (Bucsela et al., 2019, Fig. 11(c)) compared to imposing a constant amount of NO_x molecules emitted per CG lightning strike and a factor of one order of magnitude lower amount for

the emissions from IC lightning flashes. Bucsela et al. (2019) reported that LNO_x PE decreases by one order of magnitude, if the flash frequency increases by two orders of magnitude.

2   Models

2.1   Lightning NO_x production parameterization

Firstly, the relationship between the LNO_x production efficiency (PE) and the flash rate, as shown in (Bucsela et al., 2019, Fig. 11(c)), is fitted to the following equation:

$$PE = \exp\left(-a \times \log\left(f\right) + b\right), \tag{1}$$

where PE is the production efficiency in moles of NO_x per flash, f is the flash rate in kilo flashes per hour, and a and b are dimensionless fitting coefficients with values of 0.503 and 8.01, respectively. The goodness of fit for this relationship is characterized by $R^2 = 0.995$.

2.2   Climate-chemistry model and simulation set-ups

We employ the ECMWF–Hamburg (ECHAM)/Modular Earth Submodel System (MESSy version 2.55) Atmospheric Chemistry (EMAC) model (Jöckel et al., 2016) to perform pairs of five 8-year simulations using three different flash frequency parameterizations, with two different LNO_x schemes each. The simulations are conducted at a T42L90MA resolution, utilizing a quadratic Gaussian grid with box dimensions of approximately $2.8° \times 2.8°$ in latitude and longitude. The model setup covers 90 vertical levels that extend up to the 0.01 hPa pressure level, and a time step length of 720 s is employed (Jöckel et al., 2016). The lightning frequency is calculated at every time step and box by using the lightning parameterizations proposed by Price and Rind (1992), Grewe et al. (2001), or Luhar et al. (2021), being the latest a modification of the parameterization based on the CTH by Price and Rind (1992). In turn, we use scaling factors that ensure a global lightning occurrence rate of ~48 flashes per second (Christian et al., 2003; Cecil et al., 2014). We refer to Pérez-Invernón et al. (2022b) for a detailed description of the performance of the parameterizations used in EMAC. In turn, we show the simulated annual spatial distributions of lightning flash density in Figure S1. LNO_x is calculated by using a modified version of the LNOX submodel of MESSy (Tost et al., 2007). Originally, the LNOX submodel imposes a constant amount of NO_x molecules emitted per flash that can be different or equal for CG and IC lightning based on Price et al. (1997). As a second step, the LNO_x molecules are vertically distributed by following a prescribed vertical profile that can vary latitudinally or between land and ocean, following the C-shaped vertical profiles reported by Pickering et al. (1998). We modify the LNOX submodel to include the LNO_x parameterization reported by (Bucsela et al., 2019, Fig. 11(c)) and derived in Equation 1.

We conduct the simulations using the Quasi Chemistry-Transport Model (QCTM) approach (Deckert et al., 2011). The QCTM mode allows for the separation of dynamics and chemistry in order to operate the model as a chemistry-transport model. This means that minor chemical changes do not introduce noise by affecting the simulated meteorology. The overview

of the performed simulations are listed in Table 1, including the meteorological variables that serve as proxy for lightning flash frequency, the scaling factors to get ~ 48 flashes per second during 2000, and the production of LNO_x per flash and per year.

First, we perform three fully coupled free-running 8-years simulations ("BASE", where the subindex indicates the lightning flash frequency parameterization) from 1 January 2000 to 1 January 2008 to derive the forcings for the subsequent simulations. There is no consensus about the similarity or difference in the production of NO_x per flash depending on the type of lightning Schumann and Huntrieser (2007); Gordillo-Vázquez et al. (2019). However, climate-chemistry simulations usually set different LNO_x PE for CG and IC lightning (Tost et al., 2007; Jöckel et al., 2016; Gordillo-Vázquez et al., 2019). In BASE simulations, we impose a production of 1,112 mol per CG flash and 111.2 mol per IC flash, obtaining annual global emissions of LNO_x of 5.66 Tg(N)y^{-1}, 4.94 Tg(N)y^{-1} and 5.58 Tg(N)y^{-1} for the lightning parameterizations by Price and Rind (1992) (subscript P), Grewe et al. (2001) (subscript G) and Luhar et al. (2021) (subscript L), respectively. These produced amounts per flash are based on the estimation of 6.7×10^9 J per CG flash, 0.67×10^9 J per IC flash and 10×10^{16} molecules NO/J reported by Price et al. (1997). We employ the same chemical setup and chemical mechanism as detailed by Jöckel et al. (2016) for the RC1-base-07 simulations.

The second set of simulations, here referred to as control ("CTR") simulations, are similar to the BASE simulations in terms of lightning and LNO_x parameterizations, but using the radiative forcing fields from the BASE simulations, following the QCTM approach.

At this point, we explore the applicability of Equation (1) within our model. Equation (1) is derived from data aggregated over $1° \times 1°$ latitude-longitude grid boxes, whereas the simulations will be conducted using a coarser resolution of $2.8° \times 2.8°$ grid boxes. We check that the percentage of boxes that contain a flash frequency lower than a specified value in the simulation and in the gridded data of (Bucsela et al., 2019, Fig. 11(c)) are comparable. The data in Figure 1 show the total number of flashes per hour in the $2.8° \times 2.8°$ in latitude and longitude boxes from EMAC. These values were estimated by selecting all the boxes at every output timestep of 720 s (13,566,603 total samples) from the CTR simulations for the year 2000. These data allow us to ensure that the use of the LNO_x by (Bucsela et al., 2019, Fig. 11(c)) is applicable in the LNOX submodel of MESSy. According to Bucsela et al. (2019), who used the World Wide Lightning Location Network (WWLLN) mid-latitude lightning measurements corrected by the network's detection efficiency, nearly 90% of the $1° \times 1°$ boxes in latitude and longitude have flash rates lower than 2 kfl/hr, while we obtain that 90% of the $2.8° \times 2.8°$ boxes in latitude and longitude have flash rates lower than 2,225, 1,432 and 1,386 kfl/hr (Figure 1). In addition, comparison between the results of (Bucsela et al., 2019, Fig. 11(a)) and Figure 1 shows that the histogram of flashes per hour are roughly in agreement. This comparison of the instantaneous lightning frequency ensures the applicability of the LNO_x parameterization by (Bucsela et al., 2019, Fig. 11(c)) in the LNOX submodel.

The third set of simulations, here refereed to as "LNOfs" simulations, is similar to the set of CTR simulations, but using the LNO_x parameterization reported by (Bucsela et al., 2019, Fig. 11(c)), and scaling the total emissions of NO_x from Equation (1) to obtain the same total emissions of LNO_x as in the CTR simulations.

We use three lightning flash frequency parameterizations and the same LNO_x vertical profile (Pickering et al., 1998) in all the simulations to isolate the effect of the LNO_x production parameterization on the chemical composition of the atmosphere.

Table 1. Overview of the performed simulations from 1 January 2000 to 1 January 2008. The subscript indicates the used lightning parameterization: P: Price and Rind (1992), G: Grewe et al. (2001), and L: Luhar et al. (2021). The variables that serve as proxy for the lightning flash frequency are the Cloud Top Height (CTH) and the upward flux of mass (M_{up}). The scaling factors to get ~ 48 flashes per second during 2000 are included.

Simulation	Set-up	Lightning flash frequency parameterization	Variable	Scaling factor	LNO_x parameterization	LNO_x per CG/IC flash (mol per flash)	Global production of LNO_x (Tg(N)y^{-1})	Land/ocean production of LNO_x (Tg(N)y^{-1})
BASE$_P$	Fully coupled	Price and Rind (1992)	CTH	6.798	Price et al. (1997)	CG: 1,112, IC: 111.2	5.66	4.65 / 1.01
BASE$_G$	Fully coupled	Grewe et al. (2001)	M_{up}	5.851	Price et al. (1997)	CG: 1,112, IC: 111.2	4.94	3.33 / 1.61
BASE$_L$	Fully coupled	Luhar et al. (2021)	CTH	3.882	Price et al. (1997)	CG: 1,112, IC: 111.2	5.58	2.97 / 2.58
CTR$_P$	Radiative forcings fields from BASE	Price and Rind (1992)	CTH	6.798	Price et al. (1997)	CG: 1,112, IC: 111.2	5.66	4.65 / 1.01
LNOfs$_P$	Radiative forcings fields from BASE	Price and Rind (1992)	CTH	6.798	(Bucsela et al., 2019, Fig. 11(c))	CG = IC: 262	5.66	3.50 / 2.16
CTR$_G$	Radiative forcings fields from BASE	Grewe et al. (2001)	M_{up}	5.851	Price et al. (1997)	CG: 1,112, IC: 111.2	4.94	3.33 / 1.61
LNOfs$_G$	Radiative forcings fields from BASE	Grewe et al. (2001)	M_{up}	5.851	(Bucsela et al., 2019, Fig. 11(c))	CG = IC: 234	4.94	2.12 / 2.82
CTR$_L$	Radiative forcings fields from BASE	Luhar et al. (2021)	CTH	3.882	Price et al. (1997)	CG: 1,112, IC: 111.2	5.55	2.97 / 2.58
LNOfs$_L$	Radiative forcings fields from BASE	Luhar et al. (2021)	CTH	3.882	(Bucsela et al., 2019, Fig. 11(c))	CG = IC: 262	5.55	1.99 / 3.56
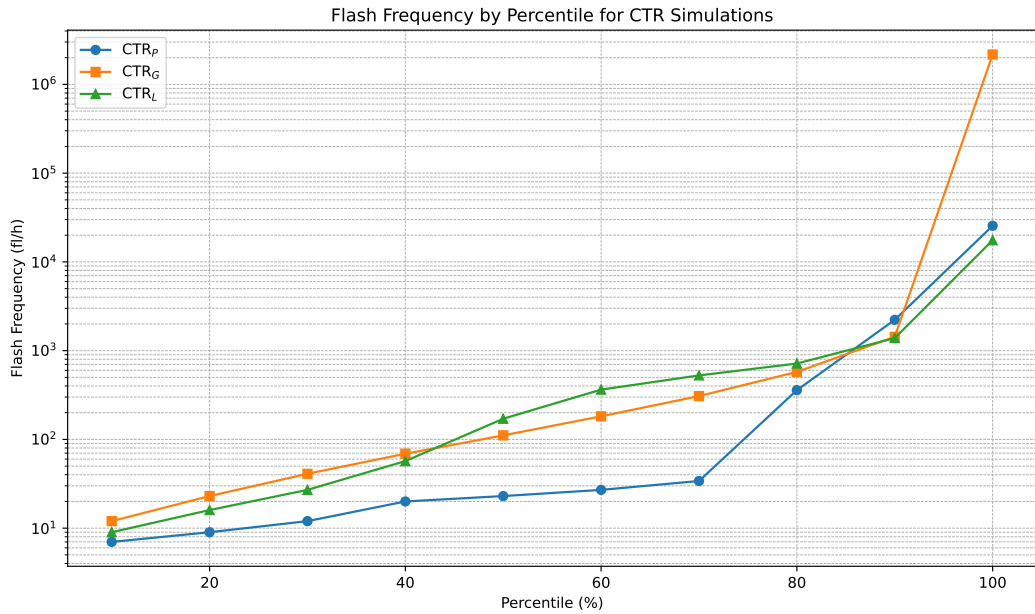
Figure 1. Fraction of $2.8° \times 2.8°$ in latitude and longitude boxes (in percentile) containing less than a given instantaneous flash frequency in flashes per hour (fl/h) from the CTR simulations.

However, other lightning parameterizations (Tost et al., 2007) and vertical profiles of LNO_x (Ott et al., 2010) can also be used, possibly producing slight variations of the results.

3 Results and discussion

3.1 Total emissions of LNO_x

We extract the global total (CG+IC) flash frequency and the total amount of LNO_x at every output time step of 720 s during 2000 to estimate the global distribution of the produced LNO_x per year from the CTR and the LNOfs simulations. Figure 2 shows the mean daily data for June-July-August (JJA) of LNO_x obtained from the CTR and the LNOfs simulations, as well as the difference between them. We select the season JJA to facilitate the comparison with OMI-WWLLN based measurements by (Bucsela et al., 2019, Fig. 3) . The LNOfs simulations predict a larger amount of LNO_x over tropical ocean, where thunderstorms have a lower lightning frequency than over land. In turn, the decrease of the production of LNO_x is larger over land in tropical regions than in mid-latitudes, as tropical thunderstorms are more active. The $LNOfs_P$ and $LNOfs_G$ simulations present a smoother distribution of the LNO_x distribution over land than the CTR_P and the CTR_G simulations, with a significant decrease of the peak production of LNO_x in North America. The difference of the land/ocean constrast of the production of LNO_x between the simulations CTR_L and $LNOfs_L$ is lower, because the parameterization by Luhar et al. (2021) detects more active thunderstorms over the oceans. In terms of the spatial distribution of LNO_x production, the parameterizations based on lightning flash frequency rates reduces differences between the three employed lightning parameterizations. The differences between the LNOfs and the CTR simulations can also be seen in the difference between the annual averaged mixing ratios of NO_x at the 800 hPa pressure level (Figure 3). The new parameterization of the production of LNO_x produces larger emissions of LNO_x over oceans, except for the high latitude oceanic regions in the $LNOf_G$ simulation, where we obtain a smaller production of LNO_x than in the CTR_G simulation. The reason of this difference is that the lightning parameterization by Grewe et al. (2001) detects more active and sparse thunderstorms in these oceanic regions than the parameterizations based on the CTH (Tost et al., 2007, Fig. 2). The spatial distribution of the mean monthly LNO_x obtained from the LNOfs simulations during 2000 is shown in Figure S2. During one complete year, the parameterizations based on the CTH ($LNOfs_P$ and $LNOfs_L$ simulations) produce a smoother spatial distribution of LNO_x, while the parameterization by Luhar et al. (2021) ($LNOfs_L$ simulation) produced relatively more LNO_x over the oceans.

When comparing Figure 2 to the mean daily LNO_x emissions during JJA as reported by (Bucsela et al., 2019, Fig. 3(c)), it becomes apparent that the LNO_x parameterization based on the lightning frequency in the LNOfs simulations produces a spatial distribution of LNO_x that aligns with space-based measurements more accurately (Bucsela et al., 2019, Fig. 3(c)) than the parameterization used in the CTR simulations. In particular, LNO_x emissions over the ocean in the CTR_P and CTR_G simulations are too low to be noticeable compared to those over land, whereas they are larger in (Bucsela et al., 2019, Fig. 3(c)). However, the $LNOf_P$ and $LNOf_G$ simulations produce significant LNO_x emissions over the oceans. Apart from that, the LNOfs simulations yield a spatial distribution of LNO_x that exhibits a more homogeneous distribution in the tropics and mid-latitudes compared to the CTR simulations.
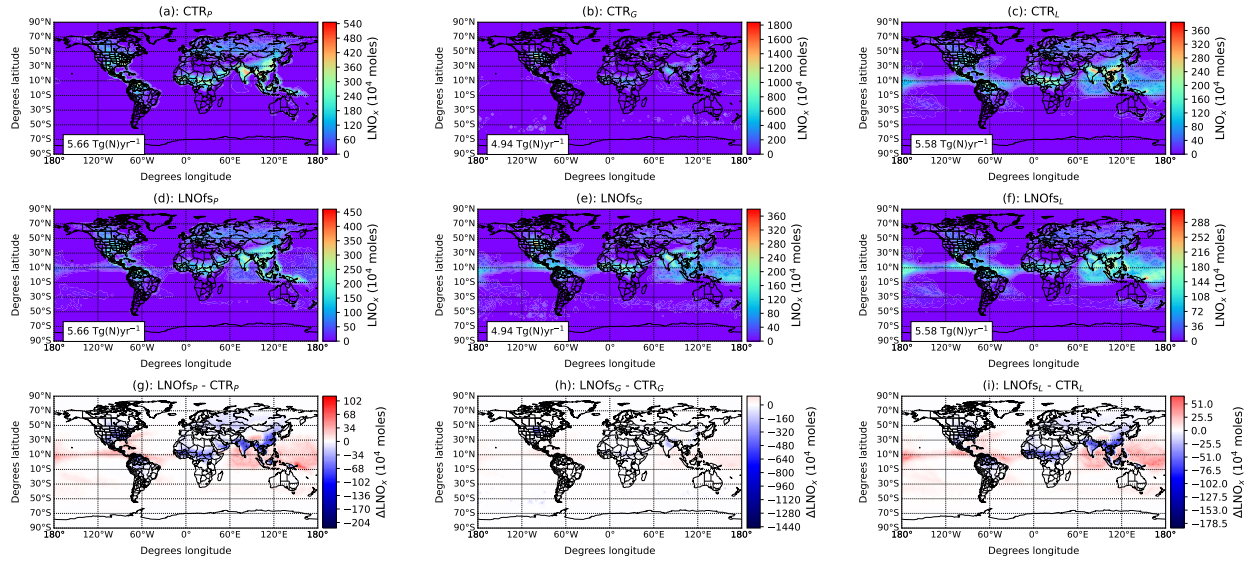
Figure 2. Daily mean LNOx production ($\times 10^4$ moles) in June-July-August (JJA) per $2.8°$ latitude $\times 2.8°$ longitude box obtained from the CTR (a-c) and the LNOfs (d-f) simulations. Panels (g-i) shows the difference between CTR and the LNOfs simulations. Note that the color scales are different in each panel.

3.2 Implications for the chemical composition of the troposphere

We compare the effect of LNO_x on the chemistry of the troposphere between the CTR and the LNOfs simulations. The spatial distributions of the annual global difference in the mixing ratio of the analyzed chemical species at the 600 hPa, 400 hPa and 200 hPa pressure level between the LNOfs and the CTR simulations are shown in the Supplemental Material (Figures S3-S11). Figures 4 and 5 show the implications of using a LNO_x parameterization based on the flash frequency in the annually and zonally averaged vertical profiles of NO_x=NO+NO$_2$, O$_3$, CO, HO_x=OH+HO$_2$, HNO$_3$ and HNO$_4$. The vertical profile of N$_2$O is not shown because the variations are negligible, as expected (absolute value lower than -0.005%). We exclude plots of LNOf$_L$ from Figures 4 and 5 because the influence of the new parameterization of LNO_x production is spatially similar to that in the LNOf$_P$ simulations but reduced in absolute value (see Figures S3-S11). The first column of Figures 4 and 5 shows the annually and zonally averaged vertical profiles of the mixing ratios of these species from the CTR$_P$ simulation, the second column shows the differences of the profiles between the LNOfs$_P$ and to the CTR$_P$ simulations, the third column shows the differences of the profiles between the LNOfs$_G$ and to the CTR$_G$ simulations, respectively.

The LNOfs simulations produce a larger mixing ratio of NO, NO$_2$ and NO$_x$ in the middle level of the tropical troposphere (around 350 hPa in Figure 4(a-i)) than the corresponding CTR simulations. However, the mixing ratio of NO$_x$ at altitudes above the 300 hPa pressure level is larger in the CTR simulations. In addition, Figure 3 indicates that the difference at the 800 hPa pressure level is larger (more positive) over the ocean, where the flash frequency in thunderstorms is lower. In turn, the differences are lower (more negative) in the lightning chimneys over land in Africa, North America and South America,

where the flash frequency is notably higher. At the 200 hPa level (Figures S9-S11(a)), the differences of NO_x mixing ratio between the LNOfs and the CTR simulations are negative in more areas. The spatial distributions of the NO_x mixing ratios in Figures S9-11(a) indicate that the mixing ratio of NO_x in the upper troposphere is lower in the LNOfs simulations, because more LNO_x is emitted in weak thunderstorms (thunderstorms with a lower flash frequency), that are less efficient in elevating the LNO_x to the upper troposphere. Therefore, the parameterization of LNO_x production based on the flash frequency (LNOfs simulations) leads to a lower contribution of lightning to the sources of NO_x of the upper troposphere compared to the CTR simulations. There are differences in the vertical profile of the variation of NO_x between the $LNOfs_P$ and $LNOfs_G$ simulations, as can be seen by comparing panels (h) and (i) in Figure 4(h,i)). Below the 500 hPa pressure level, the difference of the mixing ratio of NO_x between the simulations $LNOfs_P$ and CTR_P is positive, while the opposite is found when comparing the $LNOfs_G$ and with the CTR_G simulations. Nevertheless, these differences are small, both in absolute and in relative terms. We consider that these small differences are due to the fact that in the CTR simulations, the LNO_x depends on the CG/IC ratio, while in LNOfs simulations, both CG and IC produces the same amount of LNOx.

Differences of the NO_x mixing ratio between the LNOfs and the CTR simulations cause differences in other chemical species. The obtained differences of the mixing ratios of O_3 between the LNOfs and the CTR simulations are connected to the different spatial distributions of LNO_x production. LNO_x can produce or deplete O_3 depending on the background mixing ratio of NO_x caused by photochemistry (Crutzen, 1979; Schumann and Huntrieser, 2007; Liu, 1977; Verma et al., 2021). The NO directly produced by lightning can destroy O_3 by the chemical reaction (Levine et al., 1984)

$$NO + O_3 \rightarrow NO_2 + O_2, \tag{2}$$

and the resulting NO_2 can produce atomic oxygen by photolysis following the reaction (Levine et al., 1984)

$$NO_2 + h\nu \rightarrow NO + O. \tag{3}$$

Finally, the produced atomic oxygen can increase the mixing ratio of O_3 by interacting with a third body M as (Levine et al., 1984)

$$O + O_2 + M \rightarrow O_3 + M. \tag{4}$$

Overall, LNO_x contributes to ozone depletion in regions with low background mixing ratio of NO_x, such as over the tropical marine boundary layer. In turn, LNO_x produces ozone in regions, where the background mixing ratio of NO_x is high, such as over the continents. Figure 4(j-l) illustrates that the LNOfs simulations lead to a larger mixing ratio of ozone in the lower and middle troposphere caused by a larger production of LNO_x at these vertical levels, especially in the tropics. Additionally, the larger production of LNO_x results in very low changes of the ozone mixing ratio in the upper troposphere, due to the presence of a high NO_x background. At these higher altitudes, the efficiency of ozone production by NO_x is larger, but the emitted

LNO_x is lower. Figures S6-8(b) indicate that the larger positive change in the mixing ratio of O_3 at the 400 hPa level is located at oceanic regions, where the LNOfs simulation produces more LNO_x than the CTR simulation. In turn, the LNOfs simulations produce a lower mixing ratio of O_3 in the tropical Atlantic ocean, where the background O_3 is not produced by local oceanic thunderstorms, but by LNO_x transported from land. Figures 6-9 show the seasonal total O_3 column integrated between the ground and the top of the troposphere. During DJF, winter thunderstorms in the Northern Hemisphere are less intense than in other seasons. On the contrary, summer thunderstorms in South America and Australia are more active. This is visible in Figure 6, showing that the tropospheric column of ozone is larger over the continents in the Northern Hemisphere in the LNOfs simulations, and smaller or similar over land in South America, Australia and Southern Africa. During JJA (Figure 8), the opposite situation occurs. Winter thunderstorms over the continents of the Southern Hemisphere lead to an increase of tropospheric ozone in the LNOfs simulations, while continental summer thunderstorms in the Northern Hemisphere produce less ozone. During the MAM and SON seasons (Figures 7 and 9), lightning activity is more homogeneously distributed across the globe, resulting in the major changes in the tropospheric ozone column in the LNOfs simulations being primarily confined to land/ocean contrasts. More ozone is produced over the oceans, where less active thunderstorms produce more LNO_x than in the CTR simulations. The main difference between the $LNOfs_P$ and the $LNOfs_G$ simulations can be seen during the season DJF. During DJF, more tropospheric ozone is produced in the $LNOfs_P$ simulations compared to the CTR_P, while less tropospheric ozone is produced in the $LNOfs_G$ simulations than in the CTR_G.

The relationship between HO_x and LNO_x is not linear (Schumann and Huntrieser, 2007). Under clean air conditions and in medium polluted regions, OH is produced as a consequence of LNO_x by O_3 and NO_2 photolysis. However, in regions with large amounts of NO_x, LNO_x contributes to a depletion of the HO_2 mixing ratio by reactions between NO_2 and HO_2, contributing to a decrease of the HO_x mixing ratio. At the 600 hPa level (Figures S3-S5), where in general the background NO_x is low, increases of NO_x led to increases of HO_x (Figure 5(d-i) and Figures S3-S5). We obtain the opposite situation at the 200 hPa level, where the background NO_x is large (Figure 5(d-i) and Figures S9-S11). At the 400 hPa pressure level, where the background NO_x is medium in comparison with other vertical levels (Figure 4)(g), the relationship between the NO_x and the HO_x is more complex (Figure 5(d-i) and Figures S6-S8).

To exemplify the influence of LNO_x on the mixing ratio of HO_x, we show the impact of LNO_x on the HO_x mixing ratio in the geographical region of Europe (bounded by 42°N and 52°N degrees latitude, and 0° to 24°E degrees longitude) in Figure 10. The first panel illustrates the disparity in the hourly total column emissions of LNO_x between the $LNOfs_L$ and CTR_L simulations over a 1-year period, where negative values represent a reduced LNO_x production in the $LNOfs_L$ simulation. In the second panel, the hourly differences of the NO_x and HO_x mixing ratios at the 400 hPa level are shown. Lastly, the third panel shows the hourly background mixing ratio of NO_x at the 400 hPa level. Before day 140, when the background mixing ratio of NO_x is low, changes of NO_x and HO_x follow the same trend. Conversely, during the summer when the background mixing ratio of NO_x is large, the changes of NO_x and HO_x are of opposite signs, implying that increased NO_x leads to a decrease in the mixing ratio of HO_x.

In Figures S12 and S13, we show analogous plots to Figure 10, but at different pressure levels (200 hPa and 600 hPa, respectively). At the 200 hPa level, characterized by a large background mixing ratio of NO_x (see Figures4(g)), the changes

of NO_x and HO_x exhibit opposing behaviours. Conversely, at the 600 hPa level, where the background mixing ratio of NO_x is low (see Figures4(g)), the changes of NO_x and HO_x follow the same trend. In turn, we gather the background mixing ratio of NO_x across each cell domain at 200 hPa, 400 hPa, and 600 hPa pressure levels during hours when the changes of NO_x and HO_x share the same sign, resulting in an average mixing ratio of NO_x at 7.2×10^{-11} mol/mol. Conversely, when the changes of NO_x and HO_x are of opposite signs, the averaged mixing ratio of NO_x is 1.8×10^{-10} mol/mol. The observed disparity of the NO_x background mixing ratio under conditions of opposite sign changes confirms that the influence of LNO_x on the mixing ratio of HO_x is largely dependent on the background mixing ratio of NO_x. Additional details regarding the distribution of the background mixing ratio of NO_x under similar or opposite sign variations are shown in the Supplementary materials.

Figures 4(m-o) and 5(a-c) shows a clear inverse correlation between the variation of OH and CO, given that the CO in the troposphere is removed by OH through

$$CO + OH \rightarrow CO_2 + H. \tag{5}$$

The differences between the mixing ratios of HNO_3 and HNO_4 between the simulations can all be explained by the differences of NO_x. In the troposphere, LNO_x contributes to the production of HNO_3 and HNO_4. Therefore, in the LNOfs simulations, smaller mixing ratios of NO_x in the upper troposphere lead to lower mixing ratios of these species (Figure 5(j-o)). The global annual means shown in Figures S3-11(e,f) indicate that the reduction of HNO_3 and HNO_4 in the LNOfs simulations is larger in the upper troposphere over land, while increased mixing ratios are located over ocean.

The OH radical is a significant oxidant that reacts with methane (CH_4), influencing its atmospheric lifetime. Therefore, variations in the mixing ratio of OH caused by different parameterizations of LNO_x production can potentially affect the lifetime of CH_4. We calculate the tropospheric lifetime of CH_4 with respect to OH (τ_{CH_4+OH}) on a monthly basis using (Jöckel et al., 2016, eq. (1)). Table 2 shows the annually averaged tropospheric methane lifetime with respect to OH resulting from different simulations, together with the standard deviation. To calculate the means shown in Table2, we first compute the mean for each simulated year based on the monthly means of the 12 months. Then, we calculate the overall mean and standard deviation as the average and the standard deviation of the yearly means. At a global scale, the annually averaged lifetime of methane with respect to OH in the LNOfs simulations is reduced by 2.2%, 3.4%, and in 0.7% for the lightning parameterizations P, G, and L, respectively. We use the mean and standard deviation to compute the p-value of a two-sample t-test to assess the significance of differences in methane lifetime. A p-value threshold of 0.05 is used to determine statistical significance. The results indicate that the differences between CTR and LNOfs are significant in the P and G simulations, with p-values of 3×10^{-3} and 10^{-5}, respectively. In contrast, no significant differences are observed in the L simulations, as the obtained p-value is 0.2. In the Northern Hemisphere, the corresponding decreases are 2.5%, 6.2%, and 1.2%, respectively. In turn, we obtain decreases of 3.5%, 2.2%, and 1.5% in the Southern Hemisphere. The decreases are larger in the Southern Hemisphere, where more LNO_x is emitted due to the larger oceanic area than in the Northern Hemisphere. The new parameterization of the LNO_x production affects the lifetime of methane in the P and the G simulations more than in the L simulations. The reduction of the

Table 2. Annually averaged tropospheric methane lifetime with respect to OH (τ_{CH_4+OH}) in years and standard deviation resulting from different simulation results.

Simulation	Period	Global τ_{CH_4+OH} (y)	Northern Hemisphere τ_{CH_4+OH} (y)	Southern Hemisphere τ_{CH_4+OH} (y)
CTR$_P$	2002-2008	7.62±0.08	7.99±0.08	9.18±0.10
LNOfs$_P$	2002-2008	7.45±0.07	7.79±0.07	8.86±0.09
CTR$_G$	2002-2008	7.70±0.06	8.05±0.05	9.26±0.08
LNOfs$_G$	2002-2008	7.44±0.05	7.55±0.04	9.06±0.06
CTR$_L$	2002-2008	7.44±0.06	7.77±0.04	8.82±0.09
LNOfs$_L$	2002-2008	7.39±0.06	7.68±0.04	8.69±0.08

global methane lifetime with respect to OH deviates from that obtained by the multi-model mean 9.7±1.5 years (Naik et al., 2013).

3.3 Comparison with data of zonal ozone distribution

The simulated zonal ozone distribution from the CTR and LNOfs simulations can be compared with ozone profile data from Hassler et al. (2009) and Bodeker (2014), as previously carried out by Luhar et al. (2021), to assess the impact of different lightning parameterizations on global ozone mixing ratios. The Bodeker scientific global vertically resolved ozone database includes monthly mean vertical ozone profiles spanning from 1979 to 2016 across 70 vertical levels. In this study, we utilize the Tier 1.4 vn1.0 product, specifically the version containing the mean annual cycle derived from anthropogenic, natural, and volcanic emissions. We re-grid the data to match the resolution of the model. The comparison between the simulated seasonal zonal ozone distribution and the Bodeker scientific global vertically resolved ozone database Tier 1.4 vn1.0 product between 2002 and 2007 is shown in Figures 11-14. During all the seasons, the LNOfs simulations produce more tropospheric ozone than the corresponding CTR simulations in the tropics, causing more disagreement with measurements than the CTR simulations. The effect of the LNOfs simulations in the mid-latitude tropospheric ozone varies with the lightning parameterization and with the seasons. DJF: The new parameterization of the production of LNO$_x$ produces a larger content of tropospheric ozone in the Northern Hemisphere, contributing to produce a better agreement with measurements. In the Southern Hemisphere, the LNOfs simulations produce more tropospheric ozone in the P simulations, but less ozone in the G simulations, producing a better agreement with the measurements only in the case of the P simulations. MAM: the LNOfs$_P$ simulation shows more ozone in both hemispheres, while the LNOfs$_G$ simulations results in more ozone in the tropics but less ozone in the mid-latitudes in both hemispheres. In this case, only the LNOfs$_P$ simulations show a better agreement with the measurements, and only in the Northern Hemisphere. JJA: The LNOfs simulations result in a better agreement with observations in the Southern Hemisphere, and less agreement in the Norther Hemisphere. SON: The LNOfs simulations show a better agreement with the measured tropospheric ozone in the Southern Hemisphere, and a worse agreement in the Northern Hemisphere.

The seasonal variations in the simulated zonal ozone distribution between 2002 and 2007 (Figures 11-14) can be compared with the corresponding interannual zonally averaged differences in the vertical O$_3$ mixing ratio provided by the Bodeker Scientific Global Vertically Resolved Ozone Database (Tier 1.4, version 1.0) Hassler et al. (2009). These differences, calculated

relative to the seasonal mean for 2002–2007, are shown in Figures S26–S29. This comparison aims to evaluate the significance of the observed variations. The seasonal variations between the simulated tropospheric O_3 and the Tier 1.4 product are most pronounced in the tropics and the middle troposphere (Figures 11-14), whereas the interannual variations of the Tier 1.4 product peak in the extratropics and the upper troposphere (Figures S26–S29). Consequently, we conclude that the differences in tropospheric O_3 between the simulation and the Tier 1.4 product are relevant, since they exceed the interannual variability of tropospheric O_3.

The interannual zonally averaged differences during each season of the vertical O_3 mixing ratio between the annual Bodeker scientific global vertically resolved ozone database Tier 1.4 vn1.0 product Hassler et al. (2009) and the annually mean during the period 2002-2007 for each season are shown in Figures S26-S29.

(Jöckel et al., 2016, Fig. 29) compared the annual tropospheric partial column of ozone from the RC1-base-07 simulation with AURA Microwave Limb Sounder/Ozone Monitoring Instrument (MLS/OMI, Ziemke et al. (2011)) measurements (reproduced in Figure S30), obtaining an overestimation of ozone in the tropics, especially over Africa, Indonesia and the Indian Ocean. In turn, the RC1-base-07 simulation produced an underestimation of the tropospheric partial column of ozone below about 50°S latitude. We show in Figure 15 a comparison of the annual average tropospheric partial column of ozone between the CTR and the LNOfs simulations. The LNOfs simulations with the parameterizations based on the CTH (LNOfs$_P$ and LNOfs$_L$) produce a smaller tropospheric column of ozone in tropical Africa compared to the CTR parameterizations, resulting in a better agreement with measurements (Jöckel et al., 2016, Fig. 29). In turn, the LNOfs$_P$ and LNOfs$_L$ produce a larger column of tropospheric ozone below the 50°S latitude than the CTR simulations, leading to a better agreement with measurements. The LNOfs$_L$ simulation results in a smaller column of tropospheric ozone above 50°N latitude, showing again a better agreement with observations. However, the obtained overestimation of tropospheric ozone over the tropical oceans disagrees more with the measurements. In the case of the G simulations, the LNOfs$_G$ simulation produces a better agreement with measurements above 30°N latitude than the simulation CTR$_G$, but less agreement over the rest of the globe.

3.4 Limitations and uncertainties

In this study, we examine the impact on atmospheric chemistry of parameterizing the LNO$_x$ production based on lightning frequency. In particular, we use the global relationship between LNO$_x$ production and flash frequency as derived by (Bucsela et al., 2019, Fig. 11(c)). While substantial evidence exists, suggesting possible relationships between LNO$_x$ production per flash and flash frequency (Bucsela et al., 2019; Allen et al., 2019, 2021; Zhang et al., 2022; Pérez-Invernón et al., 2023b; Pickering et al., 2024), quantifying this relationship on a global scale using satellite-based data and global lightning measurements remains challenging and uncertain, as discussed by Bucsela et al. (2019). Firstly, it is important to emphasize that the relationship provided by Bucsela et al. (2019) was derived over mid-latitude land regions, but it is applied globally in this study. However, Allen et al. (2019) used a similar method to derive LNO$_x$ PE within the tropics (including oceans), finding that tropical PE is only 10% lower than the midlatitude PE derived by Bucsela et al. (2019). In addition, Allen et al. (2019) reported evidence for a decrease in LNO$_x$ PE with increasing flash rate on a regional basis within the tropics.

The low detection efficiency of WWLLN in some regions (Holzworth et al., 2009) together with the uncertainty of satellite-based derived vertical column density of NO_x introduce a large uncertainty of the estimated LNO_x production. Bucsela et al. (2021) used TROPOMI NO_2 and cloud measurements together with GLM lightning data to improve the estimation of LNO_x production. They reported that the relationship between the production of LNO_x per flash and the flash frequency for thunder-storms producing less than 3,000 flashes per hour and degree in America (98% of all the analyzed cases) could be weaker than the relationship reported by Bucsela et al. (2019). Therefore, the results obtained in this study should be regarded as the upper limit of the impact that an LNO_x production parameterization based on lightning flash frequency may have on the chemical composition of the atmosphere.

4 Conclusions

For the first time, a parameterization of LNO_x production, based on the flash frequency, is introduced in the climate-chemistry model EMAC. This LNO_x parameterization is based on OMI NO_2 measurements provided by Bucsela et al. (2019), who reported an inverse relationship between the lightning flash frequency in thunderstorms and the production of LNO_x per flash. Although more recent studies have reported a weaker relationship between the production of LNO_x per flash and the flash frequency in America (Bucsela et al., 2021), there are no new estimates of this relationship on a global scale. Therefore, the results obtained in this study should be considered the upper limit of the impact that an LNO_x production parameterization based on lightning flash frequency could have on atmospheric chemical composition. Six 8-years simulations by using three different lightning parameterizations (Price and Rind, 1992; Grewe et al., 2001; Luhar et al., 2021) enable us to investigate the influence of this LNO_x production parameterization for the mixing ratios of $NO_x=NO+NO_2$, O_3, CO, $HO_x=H+OH+HO_2$, N_2O, HNO_3 and HNO_4 in the troposphere.

Based on our findings, the LNO_x production parameterization based on the lightning flash frequency leads to an enhanced production of LNO_x in thunderstorms with lower flash rates compared to those that impose a constant LNO_x production rate per flash. This increase of LNO_x production in weaker thunderstorms results in less LNO_x over land and more over the oceans. In turn, more LNO_x is emitted in winter thunderstorms than in summer thunderstorms. In general, the simulations with the new parameterization of the LNO_x production lead to a spatial distribution of LNO_x that is more homogeneously distributed over the globe than the simulations with a constant LNO_x production per flash (Figure 3). As a result, we obtain a larger tropospheric column of ozone over the tropical ocean (Figures 6-9). The influence of the new LNO_x production parameterization on tropospheric ozone in other regions of the globe depends on the employed lightning flash frequency parameterization. For the lightning flash frequency parameterizations based on the CTH (Price and Rind, 1992; Luhar et al., 2021), we obtain a smaller tropospheric column of ozone over tropical Africa. In the case of the lightning parameterization based on the upward flux of mass (Grewe et al., 2001), we obtain a smaller column of tropospheric ozone at mid-latitudes in the northern hemispheres. The maximum change of the tropospheric ozone mixing ratio when using the new scheme are in the order of $\sim$3%, with the lowest variations in the case of the lightning parameterization by Luhar et al. (2021), that included already a modification of lightning frequency over oceans.

The oxidation capacity of the atmosphere is influenced by the new LNO_x production parameterization, as tropospheric NO_x plays an important role for the chemical budget of tropospheric HO_x. In particular, we obtain a global decrease of the tropospheric lifetime of methane with respect to OH ranging between 0.7% and 3.4%, especially over the Southern Hemisphere.

The new parameterization of the production of LNO_x leads to a decrease of tropospheric CO by about 2% worldwide, reaching its maximum over the tropical oceans. The mixing ratio of tropospheric HNO_3 is reduced up to 8% globally, especially over land. Finally, we obtain an increase of the tropospheric HNO_4 mixing ratio of about 4%, with significant increases over ocean and decreases over land.

These findings highlight the importance of understanding the variability of LNO_x production to enhance the chemical budget of key trace gas species in climate-chemistry models. Geostationary satellite measurements of NO_2 have the potential to significantly contribute to more accurate LNO_x production parameterizations. Examples of such satellites include the Geostationary Environment Monitoring Spectrometer (GEMS, launched in February 2020, Kim et al. (2020)), the Tropospheric Emissions Monitoring of POllution (TEMPO, launched in April 2023, Zoogman et al. (2017)), and the Meteosat Third Generation (MTG) Imaging and Sounding satellites (Holmlund et al., 2021). In particular, continuous (1-hourly) measurements of NO_2 provided by geostationary satellites over an area can offer unprecedented insight into the temporal evolution of LNO_x in thunderstorms at a quasi-global scale, revealing the relationships between LNO_x production per flash and thunderstorm evolution.

Code and data availability. The data of the simulations generated in this study have been deposited in the Zenodo repository Pérez-Invernón et al. (2024). The Modular Earth Submodel System (MESSy) (MESSy-Consortium, 2021) is continuously developed and applied by a consortium of institutions. The usage of MESSy and access to the source code are licensed to all affiliates of institutions which are members of the MESSy Consortium. Institutions can become a member of the MESSy Consortium by signing the MESSy Memorandum of Understanding. More information can be found on the MESSy Consortium website (http://www.messy-interface.org, last access: 10 Frebruary 2025). As the MESSy code is only available under license, the code cannot be made publicly available. The parameterization of LNO_x production has been developed based on MESSy version 2.55.

Author contributions. F.J.P.I.: Conceptualization, methodology, validation, formal analysis, investigation, data curation, writing—original draft. F.J.G.V, H.H. and P. J.: Conceptualization, methodology, validation, formal analysis, investigation, data curation, writing—review and editing. E. J. B.: Conceptualization, investigation, writing—review and editing.

Competing interests. At least one of the (co-)authors is a member of the editorial board of Atmospheric Chemistry and Physics.

Acknowledgements. The project that gave rise to these results received the support of a fellowship from "la Caixa" Foundation (ID 100010434). The fellowship code is LCF/BQ/PI22/11910026 (F.J.P.I.). In addition, this study is part of the project RYC2022-035821-I, funded by

MCIN/AEI/10.13039/501100011033 and FSE+ (FJPI). Additionally, this work was supported by grant PID2022-136348NB-C31 funded by MCIN/AEI/ 10.13039/501100011033 and "ERDF A way of making Europe". F.J.P.I. and F.J.G.V. acknowledge financial support from the grant CEX2021-001131-S funded by MCIN/AEI/ 10.13039/501100011033. PJ acknowledges funding from the Initiative and Networking Fund of the Helmholtz Association through the project "Advanced Earth System Modelling Capacity (ESM)" and from the Helmholtz Association project "Joint Lab Exascale Earth System Modelling (JL-ExaESM)". The content of the paper is the sole responsibility of the author(s) and it does not represent the opinion of the Helmholtz Association, and the Helmholtz Association is not responsible for any use that might be made of the information contained. The high performance computing simulations (HPC) have been carried out on the DRAGO supercomputer of CSIC.

References

Allen, D., Pickering, K. E., Bucsela, E., Van Geffen, J., Lapierre, J., Koshak, W., and Eskes, H.: Observations of Lightning NO_x Production From Tropospheric Monitoring Instrument Case Studies Over the United States, J. Geophys. Res. Atmos., 126, e2020JD034 174, https://doi.org/10.1029/2020JD034174, 2021.

Allen, D. J. and Pickering, K. E.: Evaluation of lightning flash rate parameterizations for use in a global chemical transport model, J. Geophys. Res. Atmos., 107, ACH–15, 2002.

Allen, D. J., Pickering, K. E., Bucsela, E., Krotkov, N., and Holzworth, R.: Lightning NO_x production in the tropics as determined using OMI NO_2 retrievals and WWLLN stroke data, J. Geophys. Res. Atmos., 124, 13 498–13 518, https://doi.org/10.1029/2018JD029824, 2019.

Bodeker, G.: Bodeker Scientific vertical ozone profile - mixing ratio. NCAS British Atmospheric Data Centre, last access: 27/06/2024, https://catalogue.ceda.ac.uk/uuid/11e34b5469d4813c02b31c5364995aa6, 2014.

Bruning, E. C. and MacGorman, D. R.: Theory and observations of controls on lightning flash size spectra, J. Atmos. Sci., 70, 4012–4029, https://doi.org/10.1175/JAS-D-12-0289.1, 2013.

Bucsela, E., Pickering, K., Allen, D., Loyola, D., Eskes, H., Veefkind, P., van Geffen, J., Koshak, W., and Krotkov, N.: Improved Lightning NO_x Production Estimates Using TROPOMI and GLM Data , AGU Fall Meeting 2021, held in New Orleans, LA, 13-17 December 2021., pp. A24E–07, 2021.

Bucsela, E. J., Pickering, K. E., Allen, D. J., Holzworth, R. H., and Krotkov, N. A.: Midlatitude lightning NO_x production efficiency inferred from OMI and WWLLN data, J. Geophys. Res. Atmos., 124, 13 475–13 497, https://doi.org/10.1029/2019JD030561, 2019.

Cecil, D. J., Buechler, D. E., and Blakeslee, R. J.: Gridded lightning climatology from TRMM-LIS and OTD: Dataset description, Atmos. Res., 135, 404–414, https://doi.org/10.1016/j.atmosres.2012.06.028, 2014.

Christian, H. J., Blakeslee, R. J., Boccippio, D. J., Boeck, W. L., Buechler, D. E., Driscoll, K. T., Goodman, S. J., Hall, J. M., Koshak, J. M., Mach, D. M., and Stewart, M. F.: Global frequency and distribution of lightning as observed from space by the Optical Transient Detector, J. Geophys. Res., 108, ACL 4–1, https://doi.org/10.1029/2002JD002347, 2003.

Crutzen, P. J.: The role of NO and NO_2 in the chemistry of the troposphere and stratosphere, Annual review of earth and planetary sciences, 7, 443–472, 1979.

Deckert, R., Jöckel, P., Grewe, V., Gottschaldt, K.-D., and Hoor, P.: A quasi chemistry-transport model mode for EMAC, Geosci. Model. Dev., 4, 195–206, https://doi.org/10.5194/gmd-4-195-2011, 2011.

Gordillo-Vázquez, F. J., Pérez-Invernón, F. J., Huntrieser, H., and Smith, A. K.: Comparison of Six Lightning Parameterizations in CAM5 and the Impact on Global Atmospheric Chemistry, Earth Space Sci., 6, 2317–2346, https://doi.org/10.1029/2019EA000873, 2019.

Grewe, V., Brunner, D., Dameris, M., Grenfell, J., Hein, R., Shindell, D., and Staehelin, J.: Origin and variability of upper tropospheric nitrogen oxides and ozone at northern mid-latitudes, Atmos. Environ., 35, 3421–3433, https://doi.org/10.1016/S1352-2310(01)00134-0, 2001.

Hassler, B., Bodeker, G., Cionni, I., and Dameris, M.: A vertically resolved, monthly mean, ozone database from 1979 to 2100 for constraining global climate model simulations, Int. J. Remote Sens., 30, 4009–4018, 2009.

Holmlund, K., Grandell, J., Schmetz, J., Stuhlmann, R., Bojkov, B., Munro, R., Lekouara, M., Coppens, D., Viticchie, B., August, T., et al.: Meteosat Third Generation (MTG): Continuation and innovation of observations from geostationary orbit, Bull. Am. Meteorol. Soc., 102, E990–E1015, https://doi.org/10.1175/BAMS-D-19-0304.1, 2021.

Holzworth, R. H., Rodger, C. J., Brundell, J., Jacobson, A. R., Lay, E. H., Thomas, J. N., and Weinman, J. A.: The World Wide Lightning Location Network (WWLLN): A Review and Update on Global Lightning Research, AGU Fall Meeting Abstracts, pp. A6+, 2009.

Huntrieser, H., Schumann, U., Schlager, H., Höller, H., Giez, A., Betz, H.-D., Brunner, D., Forster, C., Pinto Jr, O., and Calheiros, R.: Lightning activity in Brazilian thunderstorms during TROCCINOX: implications for NO x production, Atmos. Chem. Phys, 8, 921–953, https://doi.org/10.5194/acp-8-921-2008, 2008.

Jöckel, P., Tost, H., Pozzer, A., Kunze, M., Kirner, O., Brenninkmeijer, C. A., Brinkop, S., Cai, D. S., Dyroff, C., Eckstein, J., et al.: Earth system chemistry integrated modelling (ESCiMo) with the modular earth submodel system (MESSy) version 2.51, Geosci. Model. Dev., 9, 1153–1200, https://doi.org/10.5194/gmd-9-1153-2016, 2016.

Kang, D., Pickering, K. E., Allen, D. J., Foley, K. M., Wong, D. C., Mathur, R., and Roselle, S. J.: Simulating lightning NO production in CMAQv5. 2: evolution of scientific updates, Geosci. Model Dev., 12, 3071–3083, https://doi.org/10.5194/gmd-12-3071-2019, 2019.

Kim, J., Jeong, U., Ahn, M.-H., Kim, J. H., Park, R. J., Lee, H., Song, C. H., Choi, Y.-S., Lee, K.-H., Yoo, J.-M., et al.: New era of air quality monitoring from space: Geostationary Environment Monitoring Spectrometer (GEMS), Bull. Am. Meteorol. Soc., 101, E1–E22, https://doi.org/10.1175/BAMS-D-18-0013.1, 2020.

Koshak, W., Peterson, H., Biazar, A., Khan, M., and Wang, L.: The NASA Lightning Nitrogen Oxides Model (LNOM): application to air quality modeling, Atmos. Res., 135, 363–369, https://doi.org/10.1016/j.atmosres.2012.12.015, 2014.

Levine, J. S., Augustsson, T. R., Andersont, I. C., Hoell Jr, J. M., and Brewer, D. A.: Tropospheric sources of NO_x: Lightning and biology, Atmospheric Environment (1967), 18, 1797–1804, https://doi.org/10.1016/0004-6981(84)90355-X, 1984.

Liu, S. C.: Possible effects on froposheric O 3 and OH due to No emissions, Geophys. Res. Lett., 4, 325–328, https://doi.org/10.1029/GL004i008p00325, 1977.

Luhar, A. K., Galbally, I. E., Woodhouse, M. T., and Abraham, N. L.: Assessing and improving cloud-height-based parameterisations of global lightning flash rate, and their impact on lightning-produced NO_x and tropospheric composition in a chemistry–climate model, Atmos. Chem. Phys., 21, 7053–7082, https://doi.org/10.5194/acp-21-7053-2021, 2021.

MESSy-Consortium: The Modular Earth Submodel System, Version 2.55.2, https://doi.org/10.5281/zenodo.8360276, 2021.

Murray, L. T., Jacob, D. J., Logan, J. A., Hudman, R. C., and Koshak, W. J.: Optimized regional and interannual variability of lightning in a global chemical transport model constrained by LIS/OTD satellite data, J. Geophys. Res. Atmos., 117, https://doi.org/10.1029/2012JD017934, 2012.

Naik, V., Voulgarakis, A., Fiore, A. M., Horowitz, L. W., Lamarque, J.-F., Lin, M., Prather, M. J., Young, P., Bergmann, D., Cameron-Smith, P., et al.: Preindustrial to present-day changes in tropospheric hydroxyl radical and methane lifetime from the Atmospheric Chemistry and Climate Model Intercomparison Project (ACCMIP), Atmos. Chem. Phys., 13, 5277–5298, https://doi.org/oi.org/10.5194/acp-13-5277-2013, 2013.

Ott, L. E., Pickering, K. E., Stenchikov, G. L., Allen, D. J., DeCaria, A. J., Ridley, B., Lin, R.-F., Lang, S., and Tao, W.-K.: Production of lightning NOx and its vertical distribution calculated from three-dimensional cloud-scale chemical transport model simulations, J. Geophys. Res. Atmos., 115, https://doi.org/10.1029/2009JD011880, 2010.

Pérez-Invernón, F. J., Huntrieser, H., Erbertseder, T., Loyola, D., Valks, P., Liu, S., Allen, D. J., Pickering, K. E., Bucsela, E. J., Jöckel, P., et al.: Quantification of lightning-produced NO_x over the Pyrenees and the Ebro Valley by using different TROPOMI-NO_2 and cloud research products, Atmos. Meas. Tech., 15, 3329–3351, https://doi.org/10.5194/amt-2021-286, 2022a.

Pérez-Invernón, F. J., Huntrieser, H., Jöckel, P., and Gordillo-Vázquez, F. J.: A parameterization of long-continuing-current (LCC) lightning in the lightning submodel LNOX (version 3.0) of the Modular Earth Submodel System (MESSy, version 2.54), Geosci. Model Dev., 15, 1545–1565, https://doi.org/10.5194/gmd-15-1545-2022, 2022b.

470 Pérez-Invernón, F. J., Gordillo-Vázquez, F. J., Huntrieser, H., and Jöckel, P.: Variation of lightning-ignited wildfire patterns under climate change, Nat. Commun., 14, 739, https://doi.org/10.1038/s41467-023-36500-5, 2023a.

Pérez-Invernón, F. J., Gordillo-Vázquez, F. J., van der Velde, O., Montanyá, J., López Trujillo, J. A., Pineda, N., Huntrieser, H., Valks, P., Loyola, D., Seo, S., et al.: Lightning-Produced Nitrogen Oxides Per Flash Length Obtained by Using TROPOMI Observations and the Ebro Lightning Mapping Array, Geophys. Res. Lett., 50, e2023GL104 699, https://doi.org/10.1029/2023GL104699, 2023b.

475 Pérez-Invernón, F. J., Gordillo-Vázquez, F. J., Huntrieser, H., Jöckel, P., and Bucsela, E.: Monthly averaged lightning and trace gases data extracted from EMAC simulations (2007, T42L90MA resolution)) [Dataset], https://doi.org/10.5281/zenodo.13968463, 2024.

Pickering, K. E., Wang, Y., Tao, W.-K., Price, C., and Müller, J.-F.: Vertical distributions of lightning NO_x for use in regional and global chemical transport models, J. Geophys. Res. Atmos., 103, 31 203–31 216, https://doi.org/10.1029/98JD02651, 1998.

Pickering, K. E., Bucsela, E., Allen, D., Ring, A., Holzworth, R., and Krotkov, N.: Estimates of lightning NO_x production based on OMI

480 NO_2 observations over the Gulf of Mexico, J. Geophys. Res. Atmos., 121, 8668–8691, https://doi.org/10.1002/2015JD024179, 2016.

Pickering, K. E., Li, Y., Cummings, K. A., Barth, M. C., Allen, D. J., Bruning, E. C., and Pollack, I. B.: Lightning NOx in the 29–30 May 2012 Deep Convective Clouds and Chemistry (DC3) Severe Storm and Its Downwind Chemical Consequences, J. Geophys. Res. Atmos., 129, e2023JD039 439, https://doi.org/10.1029/2023JD039439, 2024.

Price, C. and Rind, D.: A simple lightning parameterization for calculating global lightning distributions, J. Geophys. Res., 97, 9919,

485 https://doi.org/10.1029/92JD00719, 1992.

Price, C., Penner, J., and Prather, M.: NO_x from lightning: 1. Global distribution based on lightning physics, J. Geophys. Res., 102, 5929, https://doi.org/10.1029/96JD03504, 1997.

Schumann, U. and Huntrieser, H.: The global lightning-induced nitrogen oxides source, Atmos. Chem. Phys., 7, 3823, https://doi.org/10.5194/acp-7-3823-2007, 2007.

490 Stith, J., Dye, J., Ridley, B., Laroche, P., Defer, E., Baumann, K., Hübler, G., Zerr, R., and Venticinque, M.: NO signatures from lightning flashes, J. Geophys. Res. Atmos., 104, 16 081–16 089, https://doi.org/10.1029/1999JD900174, 1999.

Tost, H., Jöckel, P., and Lelieveld, J.: Lightning and convection parameterisations – uncertainties in global modelling, Atmos. Chem. Phys., 7, 4568, https://doi.org/10.5194/acp-7-4553-2007, 2007.

Verma, S., Yadava, P. K., Lal, D., Mall, R., Kumar, H., and Payra, S.: Role of lightning NO_x in ozone formation: A review, Pure Appl.

495 Geophys., 178, 1425–1443, https://doi.org/10.1007/s00024-021-02710-5, 2021.

Wang, Y., DeSilva, A., Goldenbaum, G., and Dickerson, R.: Nitric oxide production by simulated lightning: Dependence on current, energy, and pressure, J. Geophys. Res. Atmos., 103, 19 149–19 159, https://doi.org/10.1029/98JD01356, 1998.

Wu, S., Mickley, L. J., Jacob, D. J., Logan, J. A., Yantosca, R. M., and Rind, D.: Why are there large differences between models in global budgets of tropospheric ozone?, J. Geophys. Res. Atmos., 112, https://doi.org/10.1029/2006JD007801,, 2007.

500 Wu, Y., Pour-Biazar, A., Koshak, W. J., and Cheng, P.: LNO_x Emission Model for Air Quality and Climate Studies Using Satellite Lightning Mapper Observations, J. Geophys. Res. Atmos., 128, e2022JD037 406, https://doi.org/10.1029/2022JD037406, 2023.

Zeldovich, Y., Frank-Kamenetskii, D., and Sadovnikov, P.: Oxidation of nitrogen in combustion, Publishing House of the Acad of Sciences of USSR, 1947.

Zhang, X., Yin, Y., van der A, R., Eskes, H., van Geffen, J., Li, Y., Kuang, X., Lapierre, J. L., Chen, K., Zhen, Z., et al.: Influence of convection on the upper-tropospheric O_3 and NO_x budget in southeastern China, Atmospheric Chem. Phys., 22, 5925–5942, https://doi.org/10.5194/acp-22-5925-2022, 2022.

Ziemke, J., Chandra, S., Labow, G., Bhartia, P., Froidevaux, L., and Witte, J.: A global climatology of tropospheric and stratospheric ozone derived from Aura OMI and MLS measurements, Atmos. Chem. Phys, 11, 9237–9251, https://doi.org/10.5194/acp-11-9237-2011, 2011.

Zoogman, P., Liu, X., Suleiman, R., Pennington, W., Flittner, D., Al-Saadi, J., Hilton, B., Nicks, D., Newchurch, M., Carr, J., et al.: Tropospheric emissions: Monitoring of pollution (TEMPO), J. Quant. Spectrosc. Radiat. Transf., 186, 17–39, https://doi.org/10.1016/j.jqsrt.2016.05.008, 2017.
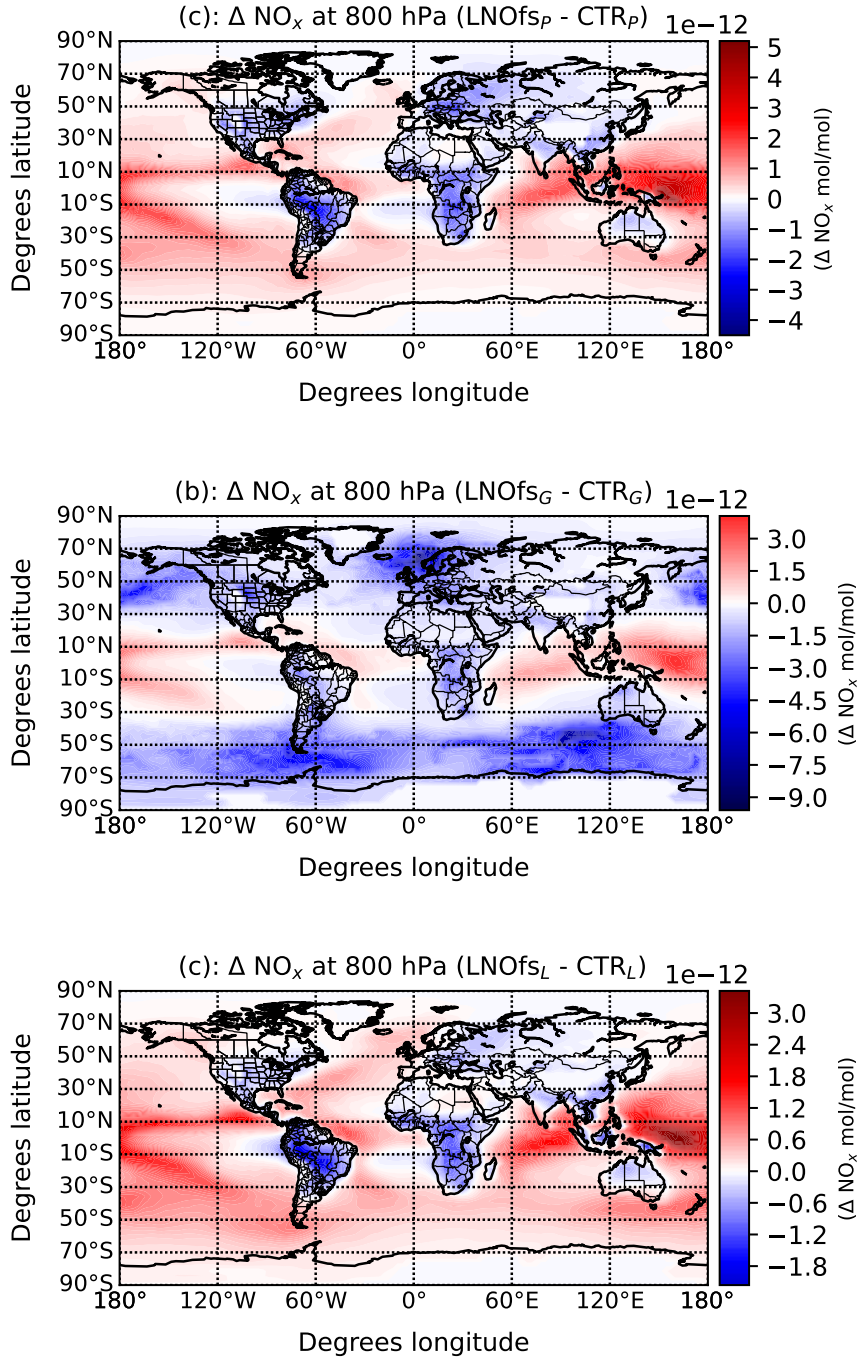
Figure 3. Annually (2002-2007) and globally averaged differences of the mixing ratio of NO_x between the simulations with the LNO_x production based on the flash frequency (LNOfs) and the simulation with a constant quantity of LNO_x production per flash (CTR) at the 800 hPa pressure level. The subscript indicates the used lightning parameterization: P: Price and Rind (1992), G: Grewe et al. (2001), and L: Luhar et al. (2021).
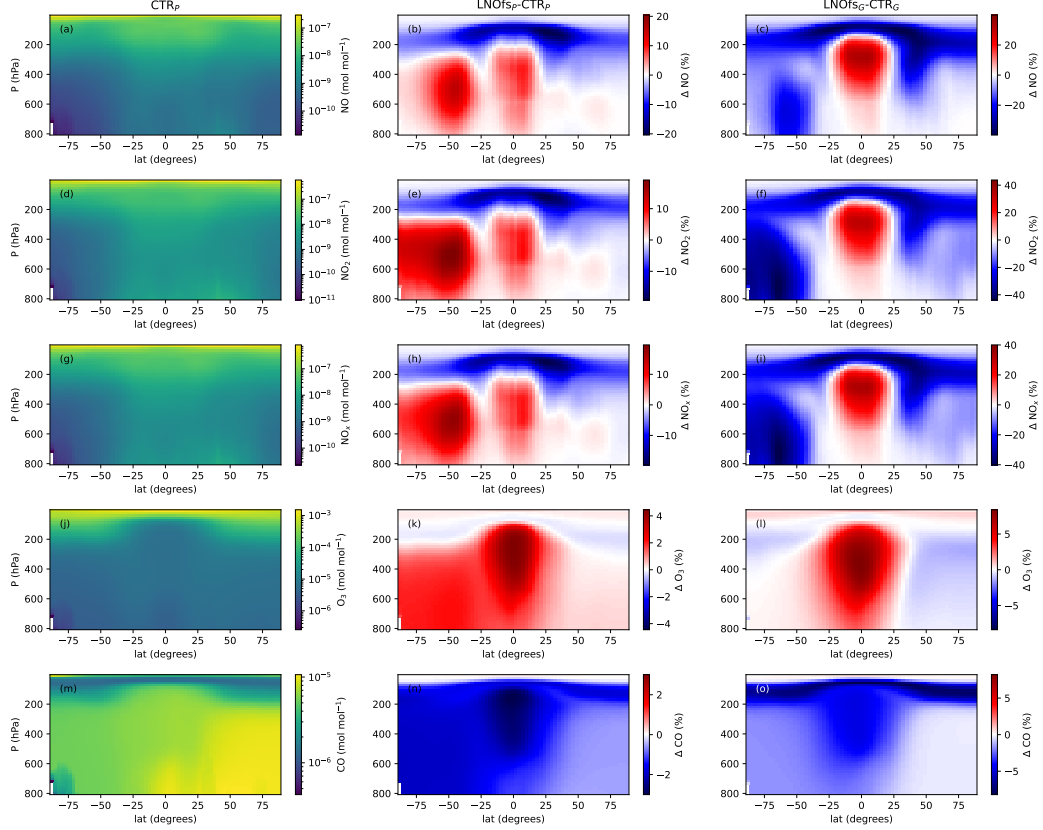
Figure 4. First column: Annually (2002-2007) and zonally averaged vertical profiles of the NO, NO_2, NO_x, O_3 and CO mixing ratios for a simulation with a constant amount of LNO_x production per flash (CTR_P). Second column: Differences (in %) between the annually and globally averaged mixing ratio of the chemical species from the simulation with the LNO_x production based on the flash frequency ($LNOfs_P$) and from the CTR_P simulation. Third column: Same as the first column but showing differences between the simulations $LNOfs_G$ and CTR_G. The differences have been calculated as $100 \times (LNOfs - CTR)/CTR$. The subscript indicates the used lightning parameterization: P: Price and Rind (1992), and G: Grewe et al. (2001).

Figure 5. First column: Annually (2002-2007) and zonally averaged vertical profiles of the OH, HO_2, HO_x, HNO_3 and HNO_4 mixing ratios for a simulation with a constant amount of LNO_x production per flash (CTR_P). Second column: Differences (in %) between the annually and globally averaged mixing ratio of the chemical species from the simulation with the LNO_x production based on the flash frequency ($LNOfs_P$) and from the CTR_P simulation. Third column: Same as the first column but showing differences between the simulations $LNOfs_G$ and CTR_G. The differences have been calculated as $100 \times$ (LNOfs - CTR)/CTR. The subscript indicates the used lightning parameterization: P: Price and Rind (1992), and G: Grewe et al. (2001).

Figure 6. Global tropospheric column of O_3 in the CTR simulations (top panels) and differences of the O_3 total column (integrated between the ground and the top of the troposphere) between the simulations LNOfs and CTR (bottom panels) averaged during DJF (2002-2007). The values are given in Dobson Units (DU). The subscript indicates the used lightning parameterization: P: Price and Rind (1992), and G: Grewe et al. (2001). The monthly total O_3 column from the CTR_L simulation can be seen in Figures S3-S14.
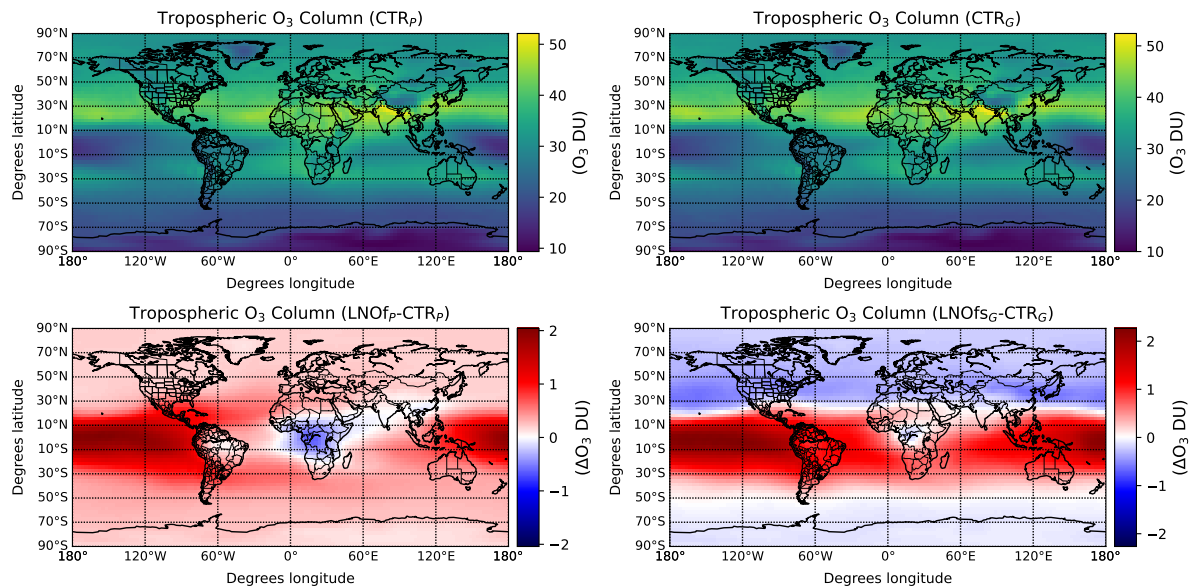
Figure 7. Global tropospheric column of O_3 in the CTR simulations (top panels) and differences of the O_3 total column (integrated between the ground and the top of the troposphere) between the simulations LNOfs and CTR (bottom panels) averaged during MAM (2002-2007). The values are given in Dobson Units (DU). The subscript indicates the used lightning parameterization: P: Price and Rind (1992), and G: Grewe et al. (2001). The monthly total O_3 column from the CTR_L simulation can be seen in Figures S3-S14.
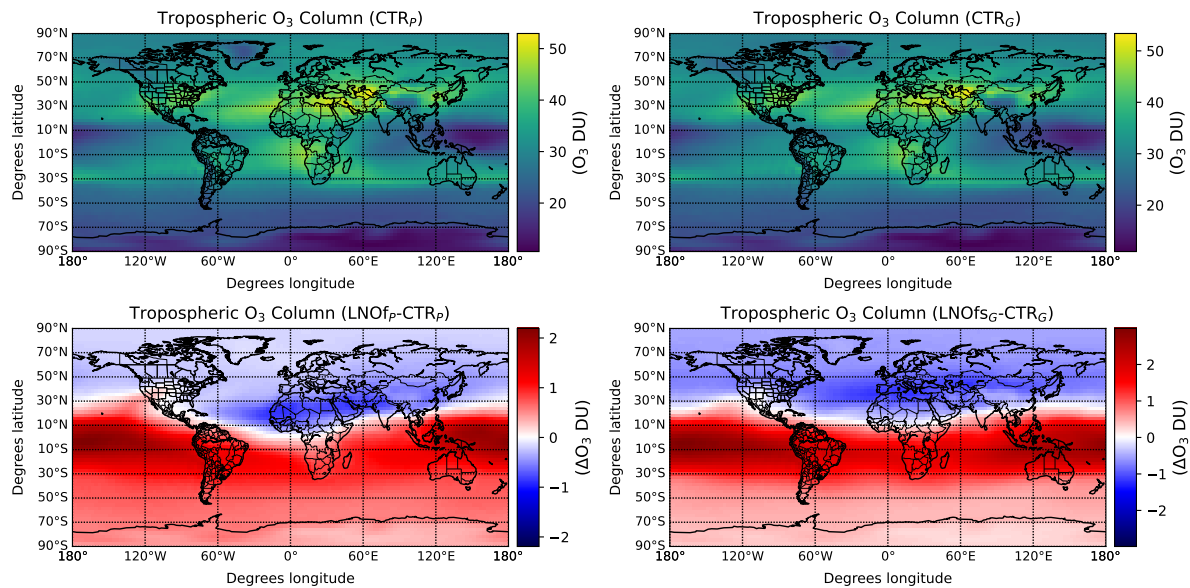
Figure 8. Global tropospheric column of O_3 in the CTR simulations (top panels) and differences of the O_3 total column (integrated between the ground and the top of the troposphere) between the simulations LNOfs and CTR (bottom panels) averaged during JJA (2002-2007). The values are given in Dobson Units (DU). The subscript indicates the used lightning parameterization: P: Price and Rind (1992), and G: Grewe et al. (2001). The monthly total O_3 column from the CTR_L simulation can be seen in Figures S3-S14.
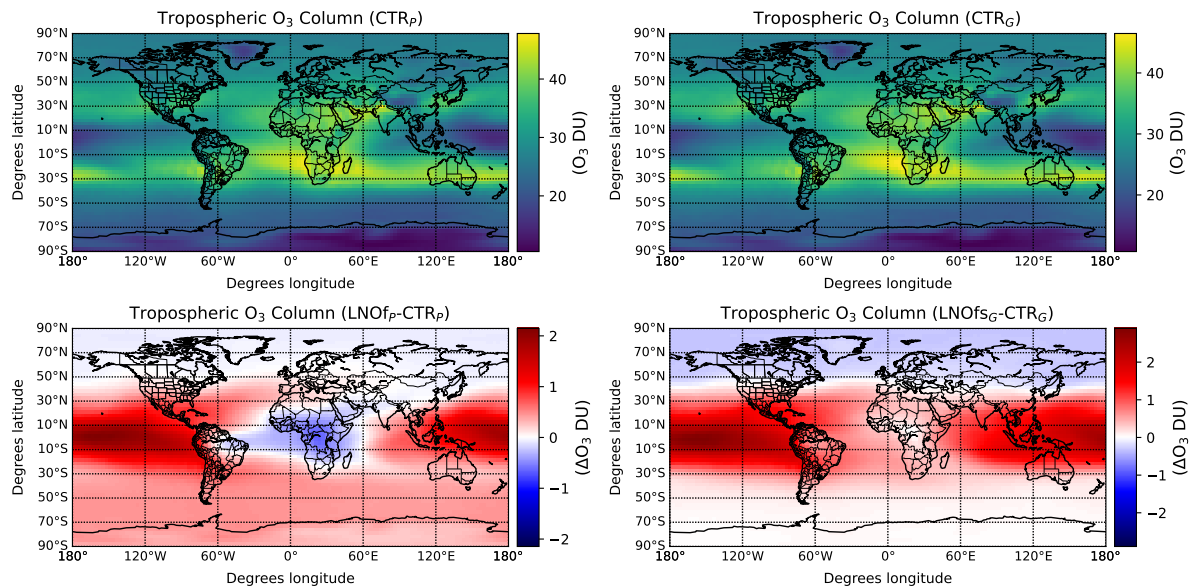
Figure 9. Global tropospheric column of O_3 in the CTR simulations (top panels) and differences of the O_3 total column (integrated between the ground and the top of the troposphere) between the simulations LNOfs and CTR (bottom panels) averaged during SON (2002-2007). The values are given in Dobson Units (DU). The subscript indicates the used lightning parameterization: P: Price and Rind (1992), and G: Grewe et al. (2001). The monthly total O_3 column from the CTR_L simulation can be seen in Figures S3-S14.
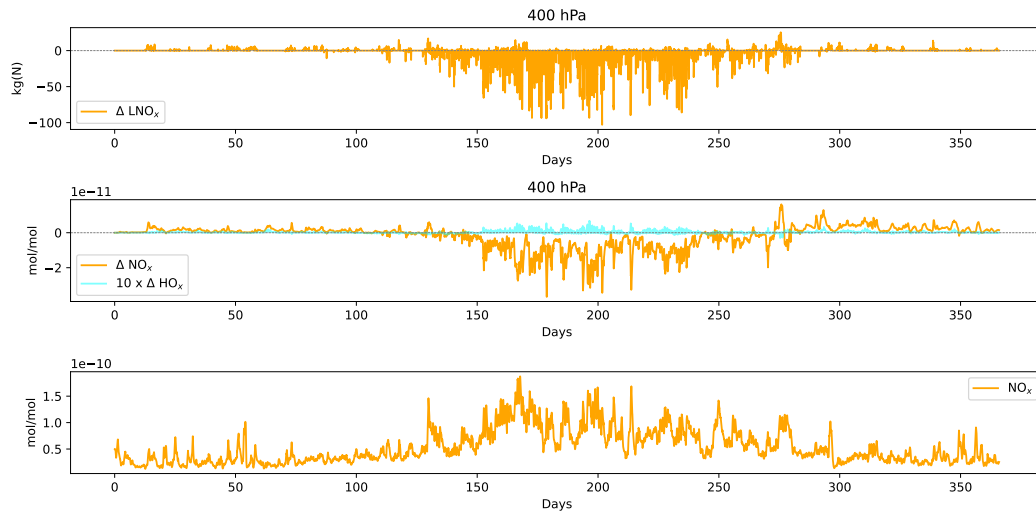
Figure 10. (Upper panel): Difference in the hourly total column production of LNO_x between the $LNOfs_L$ and CTR_L simulations over a 1-year period (day 1 corresponds to 1 January, 2000). (Middle panel): Hourly differences in the mixing ratios of NO_x and HO_x at the 400 hPa. (Lower panel): Hourly background mixing ratio of NO_x at the 400 hPa level in the $LNOfs_L$ simulation. The three panels correspond to a spatial average over Europe (bounded by $42°N$ and $52°N$ latitude degrees, and $0°$ to $24°E$ longitude degrees). The subscript P indicates the used lightning parameterization: Price and Rind (1992).
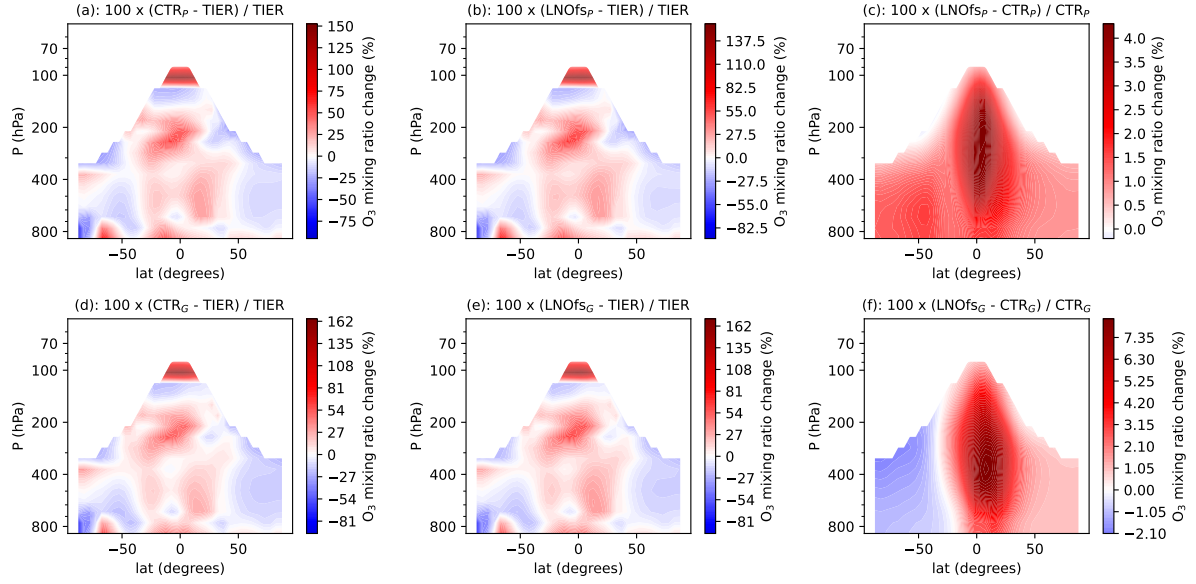
Figure 11. Seasonally December-January-February (DJF) and zonally averaged differences (in %) of the vertical O_3 mixing ratio between the simulations and the Bodeker scientific global vertically resolved ozone database Tier 1.4 vn1.0 product Hassler et al. (2009). The border with the white region represents the zonally averaged mean altitude of the climatological tropopause. The subscript indicates the used lightning parameterization: P: Price and Rind (1992), and G: Grewe et al. (2001).
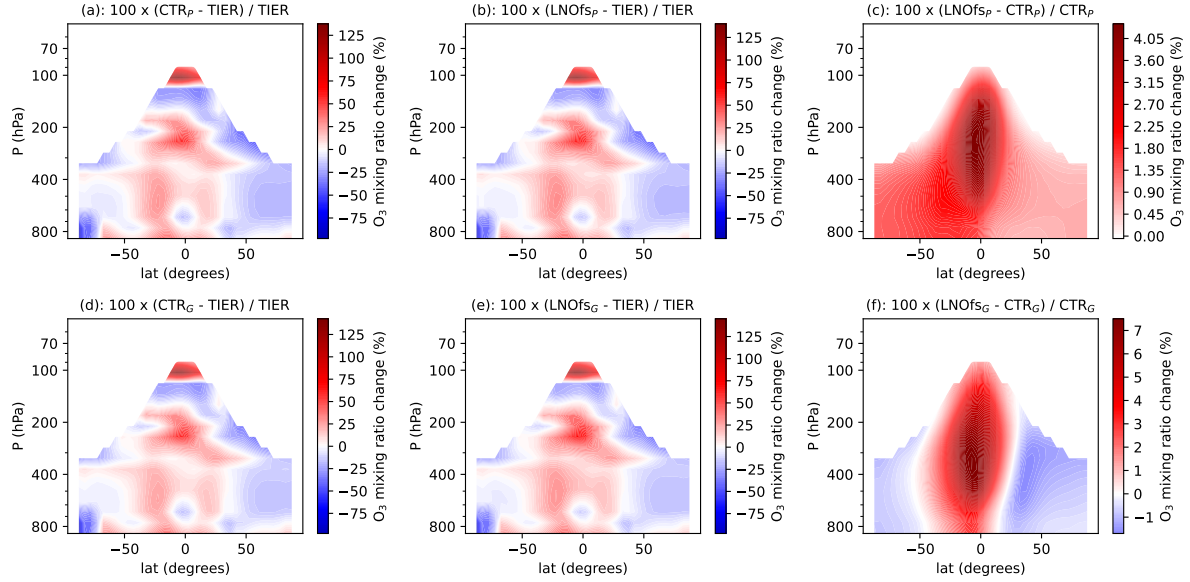
Figure 12. Seasonally March-April-May (MAM) and zonally averaged differences (in %) of the vertical O_3 mixing ratio between the simulations and the Bodeker scientific global vertically resolved ozone database Tier 1.4 vn1.0 product Hassler et al. (2009). The border with the white region represents the zonally averaged mean altitude of the climatological tropopause. The subscript indicates the used lightning parameterization: P: Price and Rind (1992), and G: Grewe et al. (2001).
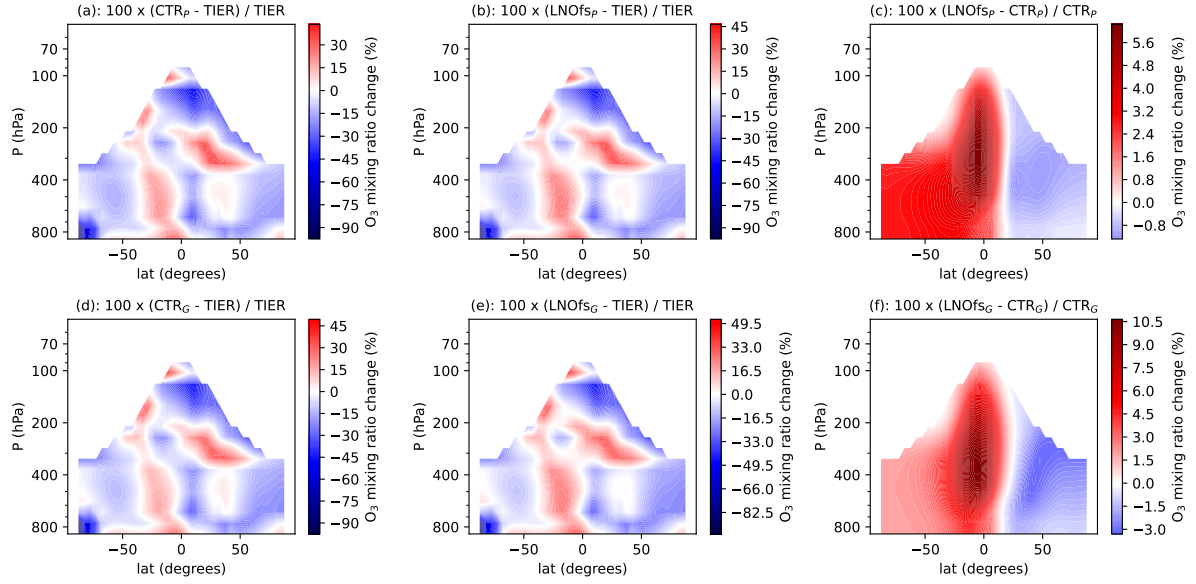
Figure 13. Seasonally (JJA) and zonally averaged differences (in %) of the vertical O_3 mixing ratio between the simulations and the Bodeker scientific global vertically resolved ozone database Tier 1.4 vn1.0 product Hassler et al. (2009). The border with the white region represents the zonally averaged mean altitude of the climatological tropopause. The subscript indicates the used lightning parameterization: P: Price and Rind (1992), and G: Grewe et al. (2001).
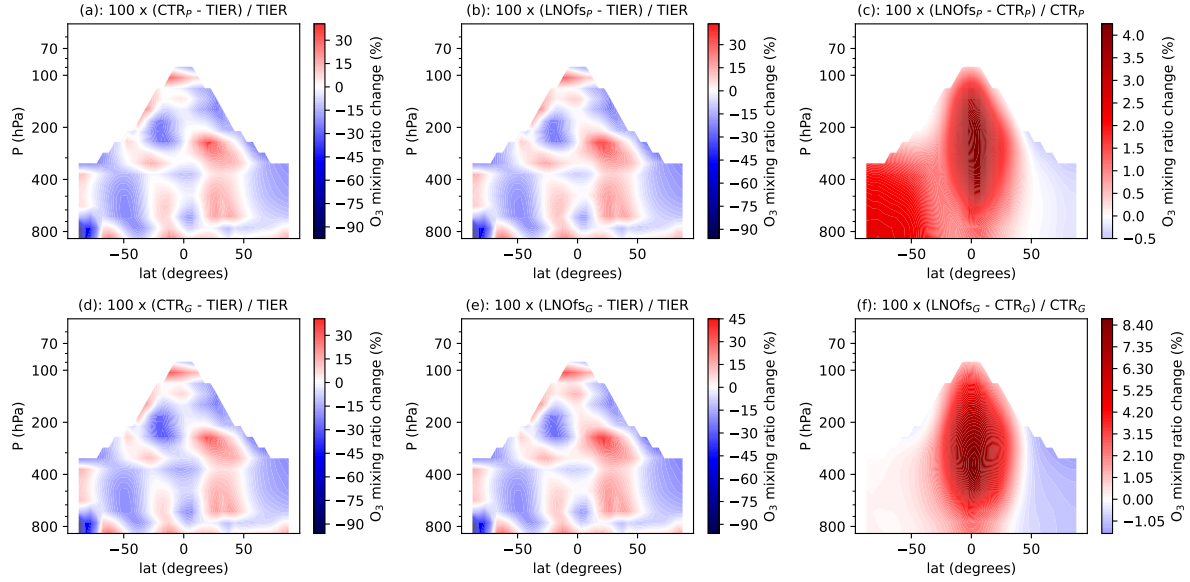
Figure 14. Seasonally September-October-November (SON) and zonally averaged differences (in %) of the vertical O_3 mixing ratio between the simulations and the Bodeker scientific global vertically resolved ozone database Tier 1.4 vn1.0 product Hassler et al. (2009). The border with the white region represents the zonally averaged mean altitude of the climatological tropopause. The subscript indicates the used lightning parameterization: P: Price and Rind (1992), and G: Grewe et al. (2001).
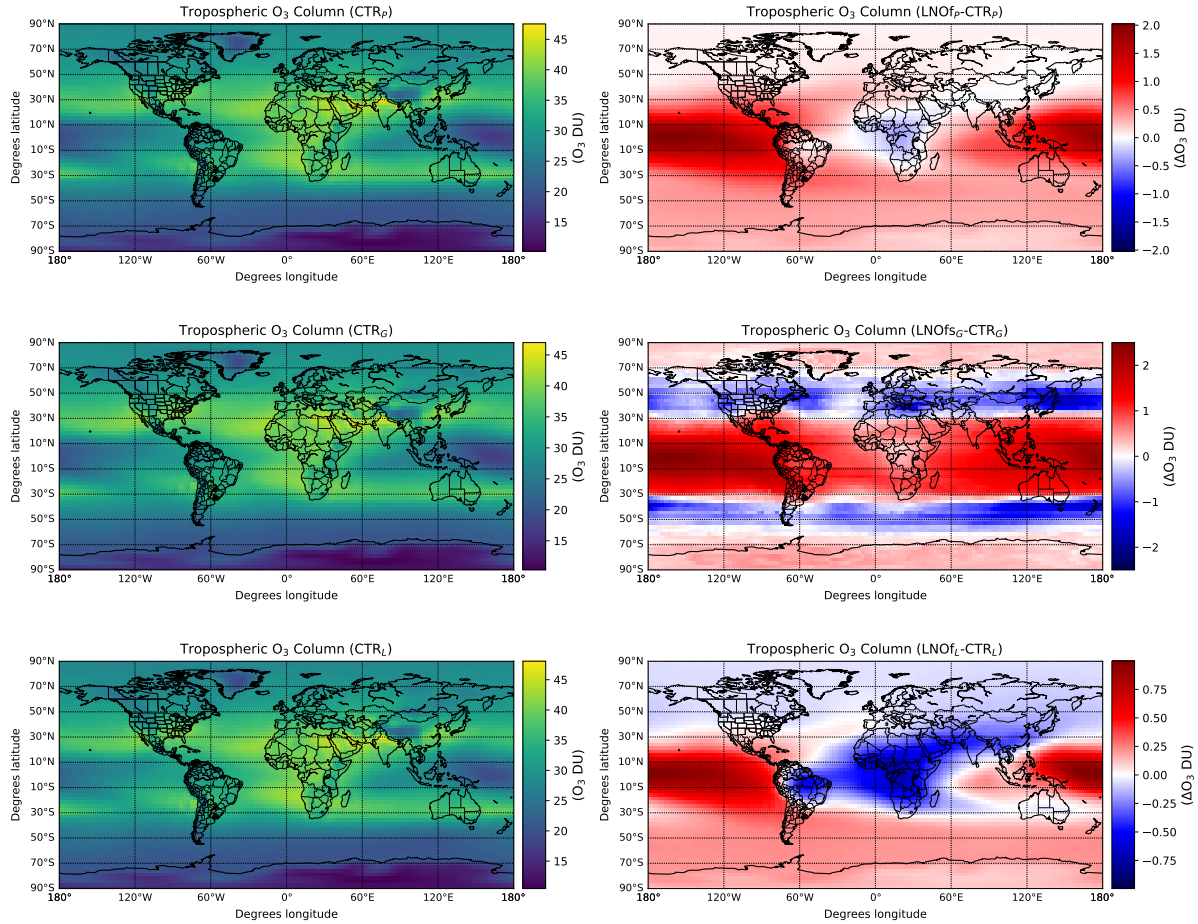
Figure 15. Annually (2002-2007) and globally averaged tropospheric column of O_3 in the CTR simulations (left panels) and differences of the O_3 total column (integrated between the ground and the top of the troposphere) between the simulations LNOfs and CTR (right panels). The values are given in Dobson Units (DU). The subscript indicates the used lightning parameterization: P: Price and Rind (1992), G: Grewe et al. (2001), and L: Luhar et al. (2021) (see Table 1). The monthly total O_3 column from the CTR_G simulation can be seen in Figures S14-S25.